Green Chemistry

View Online
Dynamic Article Links

Cite this: DOI: 10.1039/c1gc15692f

www.rsc.org/greenchem

PAPER

Magnetically separable nanocomposites with photocatalytic activity under visible light for the selective transformation of biomass-derived platform molecules

Alina M. Balu,[a] Babita Baruwati,[b] Elena Serrano,[c] Jaume Cot,[d] Javier Garcia-Martinez,[c] Rajender S. Varma*[b] and Rafael Luque*[a,b]

Received 14th June 2011, Accepted 7th July 2011
DOI: 10.1039/c1gc15692f

Novel magnetically separable TiO_2-guanidine-(Ni,Co)Fe_2O_4 nanomaterials were prepared and characterised by a series of techniques including XRD, SEM, TEM, N_2 physisorption as well as XPS and subsequently tested for their photocatalytic activities in the selective transformation of malic acid in aqueous solution. The modification with guanidine, which remarkably decreases the band gap of the metal oxide, was found to have a significant effect in the photocatalytic activity of the materials under visible light, showing a remarkably superior activity to that of the commercial Degussa P25. These materials are also envisaged to have interesting photocatalytic activities under sunlight.

1. Introduction

Photocatalytic processes have attracted a great deal of attention in recent years in our aim to switch to more benign, atom efficient and sustainable processes that make use of environmentally friendly reagents under mild conditions.[1–3] Heterogeneous photocatalysis can indeed offer a significant versatility to assist scientists in finding the appropriate solutions for key issues affecting our society (*i.e.* energy issues). This versatility is reflected in the remarkable number of applications which have been to oxidations and oxidative breaks (*i.e.* removal of organic pollutants from wastewater), reductions, isomerizations, substitutions, condensations and polymerizations.[2–5]

In general, an ideal photocatalyst should feature photostability under the source of irradiation, a chemical and/or biological inert nature, low cost and availability and most importantly the capability to adsorb reactants under efficient photonic activation ($h\upsilon \geq E_g$) as well as being as much selective as possible in the target reaction.[3,6]

Nanometric size TiO_2 has been widely employed as photocatalyst in many of these previously mentioned processes due to its inherent ability of generating charged carriers, thereby inducing reductive and oxidative processes.[7] It also has a high photocatalytic activity, low toxicity, chemical stability and very low cost.[8] The anatase form of titania has been reported to give the best combination of photoactivity and photostability.[4] Practically, TiO_2 photoactivation takes place in the range of 300–388 nm.

Nevertheless, there are important drawbacks that severely limit the application of titanium dioxide photocatalysts as such to degrade organic pollutants in the gas or liquid phase and/or to perform useful transformations of organic compounds.[1,9,10] One of its most important limitations is the lack photocatalytic activity under visible light.[11,12]

The anatase form of TiO_2 is a wide band gap semiconductor (3.2 eV bandgap in most media), corresponding to an onset of the optical absorption band at about 350 nm. This onset of the TiO_2 absorption is also inadequate to achieve efficient solar-light photocatalytic activity (only *ca.* 5% of the solar light energy can be absorbed by TiO_2).

In view of these premises, there has been a continued interest in improving the photocatalytic efficiency of TiO_2 catalysts for visible and/or sunlight irradiation[13] by different strategies, namely the use of an organic dye as photosensitizer[14] or its modification and/or doping with metallic[15] and non-metallic elements.[11,16] Asahi *et al.* firstly showed an absorption increase of TiO_2 in the visible region upon nitrogen doping,[11] paving the way to further studies of titania doping with non-metallic elements including C and S. Doping with these elements rendered TiO_2 materials that were able to work under visible light.[17]

[a]*Dpto. Química Orgánica, Universidad de Córdoba, Campus de Rabanales, Edif. Marie Curie, Ctra. Nnal. IV, Km 396, E-14014, Córdoba, Spain. E-mail: q62alsor@uco.es*
[b]*Sustainable Technology Division, National Risk Management Research Laboratory, US Environmental Protection Agency, MS 443, 26 West Martin Luther King Drive, Cincinnati, Ohio, 45268, USA. E-mail: Varma.Rajender@epamail.epa.gov*
[c]*Molecular Nanotechnology Lab, Department of Inorganic Chemistry, University of Alicante, Ctra. San Vicente s/n, E-03690, Alicante, Spain*
[d]*Institut de Química Avançada de Catalunya CID-CSIC, C/Jordi Girona 18 -26, 08034, Barcelona*

Another important issue of current photocatalytic research is related to the efficient separation of the catalyst upon reaction completion.[18] Generally, conventional photocatalysts need an additional filtration (settling) step and/or tedious workup to be recovered from the reaction mixture that often leads to loss of catalyst (due to its fine particles in the nanometre scale) and difficulties in separation. Despite several reports that deal with the immobilisation of the photocatalysts onto various supports (*e.g.* beads, zeolites, carbons),[19] this stabilisation rendered less efficient and therefore active catalysts due to a reduction in their effective surface areas and reduced mass-transfer rates.

The design of magnetically separable catalysts is envisaged to be a promising alternative to improve the efficient separation of photocatalysts from solutions by applying a simple magnet, meeting both the requirements of high accessibility with improved reusability.[20] The combination of these features with TiO_2 can also offer important alternative nanomaterials which find applications in a wide range of reactions due to their potential in designing surface functionalities along with catalyst preparation.[21–23] For more information, please refer to recently reported revisions of the topic by Cozzoli *et al.*[24,25]

Following our initial work in both the preparation of magnetically separable catalysts[26,27] and visible-light N-doped photocatalysts,[28,29] herein, we report a simple methodology for the preparation of magnetically separable N-modified TiO_2-(Ni,Co)Fe_2O_4 materials. These materials combine the advantage of being easily recoverable by using a simple magnet as well as offering the possibility to work under visible and sunlight irradiation. The activity of the materials was tested in the selective photocatalytic transformation of 2-hydroxy-butandioic acid (malic acid) in aqueous solutions to C1 and C2 chemicals. Selective oxidation catalysts are of utmost importance in heterogeneous photocatalysis as these reactions tend to generate a series of byproducts along with the target compound, especially in photocatalytic processes where the photo-transformation often leads to complete mineralisation of the starting material.[30]

2. Experimental

All chemicals are purchased from Aldrich Chemicals and are used without further purification.

2.1. Synthesis of materials

Synthesis of the TiO_2 guanidine nitrate (TiO_2-G) [non magnetic]. In a typical procedure, 20 g of $TiCl_4$ (digested to 50% in HCl) was added to 1000 mL of water. 80 g of guanidine nitrate was then added to the solution and magnetically stirred for 30 min. An ammonium hydroxide solution was then added to increase the pH of the solution to 9. The reaction was continued at room temperature for 24 h. The ensuing precipitate was then centrifuged and washed with water three times to remove the chlorides and any other water-soluble reactants. The product was then dried at 100 °C overnight, powdered, and calcined at 350 °C to obtain the final bright yellow colored products.

A commercial Degussa P25 catalyst (Aeroxide® TiO_2, Sigma–Aldrich) was also characterised and subsequently utilised for comparative purposes.

Procedure for the preparation of the magnetically separable photocatalysts TiO_2-G-(Ni, Co)Fe_2O_4. The catalysts (identical procedure for Ni and Co) were prepared in two steps, namely the preparation of the magnetic nanoparticle support (nanoferrites) and subsequent deposition of the N-modified titanium dioxide. A typical procedure for the preparation of the TiO_2-G-$NiFe_2O_4$ material was as follows:

(a) Synthesis of $NiFe_2O_4$ nanoparticles. 2.28 g Ni $(NO_3)_2$ $6H_2O$ and 6.88 g Fe $(NO_3)_3 9H_2O$ was dissolved in 200 mL of deionized water. Ammonium hydroxide (25%) was added into the solution to bring the pH up to 9 under magnetic stirring. The mixture was then further stirred for 1 h at room temperature and transferred to a Teflon lined stainless steel autoclave. The temperature of the autoclave was then raised to 220 °C at a rate 10 °C min^{-1} and maintained at that temperature for 2 h. The reaction mixture was then cooled to room temperature, filtered off, washed 3 times with water and dried overnight in an oven at 100 °C to yield the $NiFe_2O_4$ nanoparticles.

(b) Synthesis of the TiO_2-G-$NiFe_2O_4$ catalyst. 2.1 g $NiFe_2O_4$ nanoparticles were dispersed in 1000 mL deionized water by ultrasonication for 1 h in order to break up the aggregates that might have formed during the processing steps. 40 mL (50% in HCl) $TiCl_4$ and 80 g guanidine nitrate were then added. The mixture was stirred for 15 min and then ammonium hydroxide (25%) was added to hydrolyse the mixture bringing the pH up to 9. The nucleation and growth of the TiO_2 particles on the surface of the magnetic nanoparticles restricted them from agglomeration during the stirring process, in a similar way as previous reports for other supported nanoparticles.[31] The mixture was then stirred magnetically overnight, filtered off, washed several times with water and dried overnight in the oven at 100 °C. The powder eventually obtained was calcined at 350 °C for 2 h to give the final TiO_2-G-$NiFe_2O_4$ catalyst.

The TiO_2-G-$CoFe_2O_4$ material was synthesized using an identical methodology to that of the $NiFe_2O_4$-TiO_2-G changing the precursor to $Co(NO_3)_2$ $6H_2O$.

2.2. Materials characterization

The phases of the as-synthesized catalysts were determined by X-ray diffraction in an MMS X-ray diffractometer with a Cu-Kα source in the 2θ range 20° to 80°. The data were collected with a step of 1 K min^{-1}. A few drops of the as-synthesized nanoparticles in isopropyl alcohol were added to a quartz plate and dried at room temperature before recording the X-ray patterns.

Nitrogen physisorption was measured with a Micromeritics instrument model ASAP 2000 at −196 °C. The samples were outgassed for 2 h at 100 °C under vacuum ($P < 10^{-2}$ Pa) and subsequently analyzed. The linear part of the BET equation (relative pressure between 0.05 and 0.22) was used for the determination of the specific surface area. The pore size distribution was calculated from the adsorption branch of the N_2 physisorption isotherms and the Barret-Joyner-Halenda (BJH) formula. The cumulative mesopore volume was obtained from the PSD curve.

TEM micrographs were recorded on a Phillips CM 20 TEM microscope at an operating voltage of 200 kV. A drop of the as-synthesized nanoparticles in ethanol was loaded on a carbon

coated copper grid and then allowed to dry at room temperature before recording the micrographs.

UV-DRS spectra were recorded on a Shimadzu UV-250IPC instrument in the 200 to 800 nm range.

XPS measurements were performed in a ultra high vacuum (UHV) multipurpose surface analysis system (SpecsTM model, Germany) operating at pressures $<10^{-10}$ mbar using a conventional X-ray source (XR-50, Specs, Mg-Kα, 1253.6 eV) in a "stop-and-go" mode to reduce potential damage due to sample irradiation. The survey and detailed metal high-resolution spectra (pass energy 25 and 10 eV, step size 1 and 0.1 eV, respectively) were recorded at room temperature with a Phoibos 150-MCD energy analyser. Powdered samples were deposited on a sample holder using double-sided adhesive tape and subsequently evacuated under vacuum ($<10^{-6}$ Torr) overnight. Eventually, the sample holder containing the degassed sample was transferred to the analysis chamber for XPS studies. Binding energies were referenced to the C 1s line at 284.6 eV from adventitious carbon.

The magnetic properties of the nanomaterials were recorded on a Lakeshore 7000 vibrating sample magnetometer (VSM) up to a field of 10 000 G at room temperature.

2.3. Photocatalytic experiments

All catalytic tests were performed in a Pyrex cylindrical double-walled immersion well reactor open to air. In a typical experiment (see Fig. 7 for more details), an aqueous solution (50 mL) containing 0.5 mmol malic acid and 0.1 g catalyst was maintained in the dark for 1 h (to reach complete adsorption at equilibrium) and subsequently exposed to a 150 W Quartz Halogen Lamp (Fiber-Lite, Dolar Jenner Industries), which produces strong visible light ($\lambda > 400$ nm) to start the photocatalytic reaction. An adequate UV-filter to remove most of the emission before 400 nm was utilised in the reaction (to use P25 as comparison in the photocatalytic reaction). Under these conditions, a very low conversion of P25 (which does not absorb in the visible range) was obtained. A water bath was used to maintain the solution at RT (25 °C). Samples were periodically withdrawn (every 0.25 h) and analysed by HPLC, GC and GC/MS. Dark experiments (in the absence of visible light) were carried out in a similar way to those under visible light, providing no conversion of starting material after 2 h reaction.

Total mineralisation was followed by measuring the total organic carbon (TOC) at different times in solution. Under optimised conditions, a >98% mineralisation was obtained after 12 h and TOC of actual experiments performed (0.5–2 h) was found to be over 90% of the initial content (less 10% mineralisation).

3. Results and discussion

The corresponding X-ray diffraction pattern for the as-synthesized TiO_2-G sample correlated well with that of a pure anatase form (Fig. 1). Crystallite sizes as calculated using the Scherrer equation were found to be 6.77 nm, in good agreement to the particle size obtained from TEM measurements (Fig. 2, bottom).

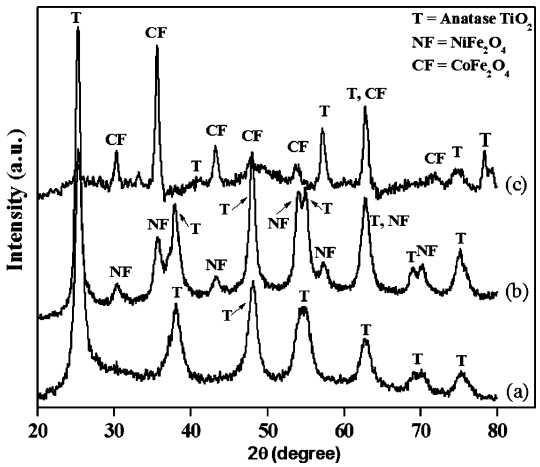

Fig. 1 XRD pattern of the TiO_2-G catalyst showing the clear diffraction pattern of the anatase phase (a) as well as of TiO_2-G-$NiFe_2O_4$ (b) and TiO_2-G-$CoFe_2O_4$ (c).

The magnetically separable materials synthesized from TiO_2-G did not correspond to a single phase compound but confirmed to be a mixture of Ni Fe_2O_4 or $CoFe_2O_4$ and TiO_2 by X-ray diffraction and TEM (TiO_2-G was growth and deposited on the surface of the Ni or Co ferrite nanoparticles, the obtained photocatalyst being N-modified titanium dioxide nanoparticles supported on the ferrites). Fig. 1 also shows the corresponding X-ray diffraction patterns for the as synthesized samples in which the typical diffractions of the anatase phase (T)[32] and the respective nanoferrites ($NiFe_2O_4$, $CoFe_2O_4$)[33] are depicted. No other TiO_2 phase contamination (rutile, brookite) was observed in the synthesized materials. The Scherrer equation gives a nanoparticle size of 5.99 nm ($NiFe_2O_4$ particle) and 11.9 nm (TiO_2) for TiO_2-G-$NiFe_2O_4$ as well as 8.3 nm ($CoFe_2O_4$ particle) and 12 nm (TiO_2-G-$CoFe_2O_4$), respectively, in good agreement with those observed in the TEM micrographs (Fig. 2, top images). These show that the particles are in the 5–10 nm range with a very narrow size distribution and a slight aggregation for both the TiO_2-G and the magnetically separable nanomaterials, respectively. The aggregation might have occurred in the absence of any coating agent or organic moieties on the surface of the particles. The larger size of the TiO_2-(Ni or Co)Fe_2O_4 materials as compared to TiO_2-G correlates well with the deposition of the TiO_2-G phase on the nanoferrites (thus increasing nanoparticle sizes in the final photocatalysts).

The morphology of the materials is quasi-spherical as found in SEM micrographs (Fig. 3), which was almost identical regardless of the preparation method for both non magnetic and magnetically separable catalysts.

Textural properties of the materials are summarised in Table 1. As compared to the commercial TiO_2 P25, the synthesized materials possessed significantly higher surface areas (>200 m^2 g^{-1}) and a narrow pore size distribution (5–6 nm).

UV-DRS spectra of the synthesized sample clearly shows the extension of the absorption band to the visible region (Fig. 4). The TiO_2-G sample has two broad absorption bands at 390 nm and 462 nm respectively, as well as a very small contributions at *ca.* 550 nm, clearly pointing to a potential photocatalytic activity under visible light. The intense yellow colour of the N-modified titania materials can therefore be ascribed to the N-doping, in

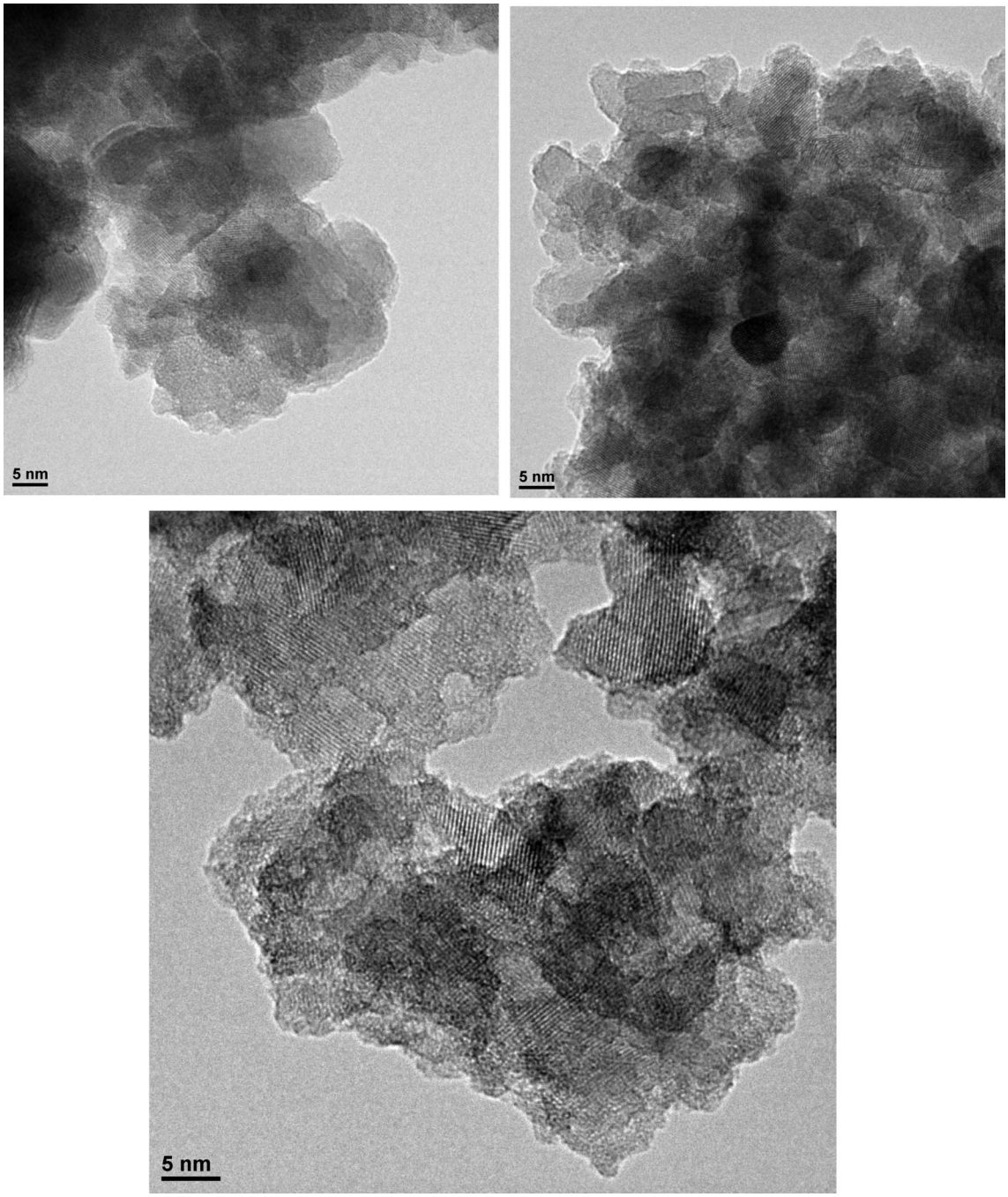

Fig. 2 TEM micrographs of TiO_2-G-$CoFe_2O_4$ (top, left) and TiO_2-G-$NiFe_2O_4$ (top, right) as compared to the parent TiO_2-G (bottom) catalyst.

good agreement with previous reports.[28,34,35] Comparatively, P25 only exhibited the fundamental absorption edge of TiO_2 at *ca.* 387 nm, showing negligible absorption in the visible range.[34] UV spectra of the magnetically separable catalysts shows a continuous absorption from the visible to the UV range. This is due to the coloured ferrite particles which absorb throughout the visible range.

XPS analysis was subsequently employed to determine the chemical states and elements present in the materials. Fig. 5 depicts the survey spectra of the TiO_2-G and TiO_2-G-$NiFe_2O_4$ materials, showing the presence of Ti, O, N, C and traces of Cr (as potential impurity present in the Ti precursor) in both materials as well as appreciable traces of Cl in the magnetically separable composites, which were not observed in the TiO_2-G, coming from the $TiCl_4$ utilised as titania precursor in the synthesis procedure.

O 1s XP spectra of the different materials are shown in Fig. 6. Four distinctive peaks can be observed in the TiO_2-G spectrum. The peak at 529.9 eV is the characteristic peak of the Ti–O bond in TiO_2, corresponding to around 50% of the O species in the material, while the peak at *ca.* 531.2 eV has been reported to be due to N–Ti–O species,[36] accounting in this case for over

Table 1 Textural properties of various TiO_2 modified materials

Material	d_p[a] (nm)	A_{BET}[b] ($m^2\ g^{-1}$)	V_p[c] ($cm^3\ g^{-1}$)
TiO_2 P25 (Aeroxide® P25)	21	50	0.30
TiO_2-G	5.0	280	0.35
TiO_2-G-$NiFe_2O_4$	4.9	217	0.30
TiO_2-G-$CoFe_2O_4$	5.8	200	0.31

[a] Average mesopore diameters were estimated from the adsorption branch of the nitrogen isotherm using the BJH method. [b] The BET surface area was estimated by using multipoint BET method using the adsorption data in the relative pressure (P/P_0) range of 0.05–0.22. [c] Cumulative mesopore volume obtained from the PSD curve.

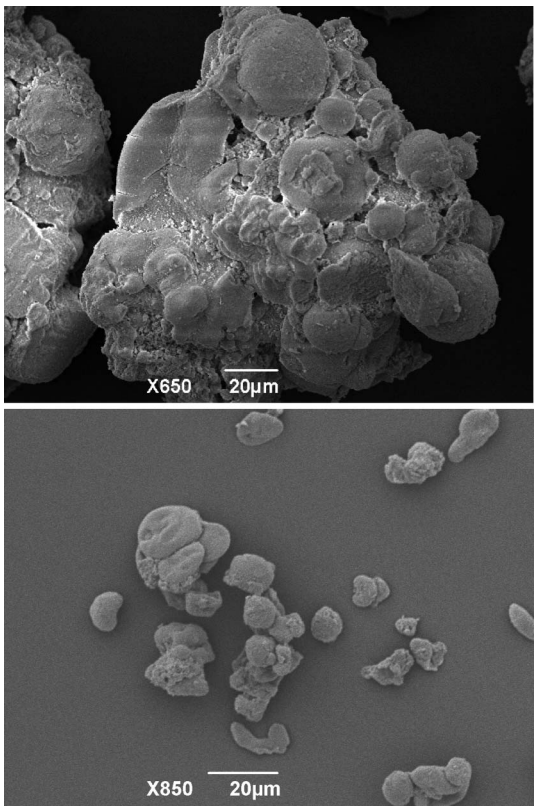

Fig. 3 SEM micrographs of TiO_2-G-$NiFe_2O_4$ (top) as compared to TiO_2-G (bottom).

35% of the total O species. An additional peak appears at *ca.* 527.7 eV (10% O species) and could be attributed to Ti–O–N species in the materials,[36] most probably established between the hydroxyl groups of TiO_2 and the functional N atoms of guanidine (terminal NH_2 groups). Last, the small contribution at 532.1 eV (<5% of O species) can be assigned to a different type of N–Ti–O environment to that observed at 531.2 eV, which could be due to the linkage of a different N from guanidine (N from the imine part of the molecule). Interestingly, the O 1s spectra of TiO_2-G-(Ni or Co)Fe_2O_4 were very similar to that of TiO_2-G, which indicates the N-TiO_2 phase is the main phase present in the surface of the materials. This finding is also in good agreement with the observed deposition of the TiO_2-G phase on the nanoferrites as confirmed by XRD. Particularly, the TiO_2-G-$NiFe_2O_4$ material exhibited a higher contribution of the characteristic Ti–O bond in titania (>60%) and a significantly

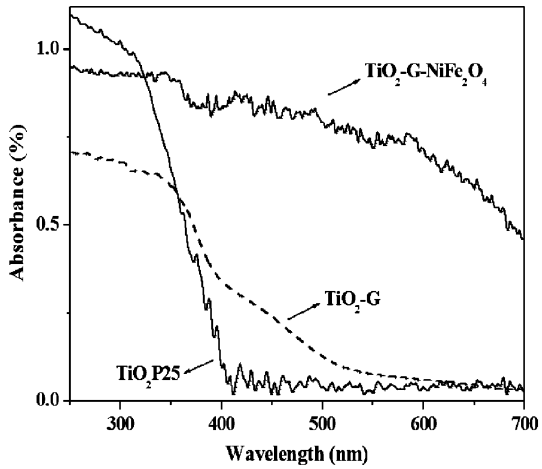

Fig. 4 UV-DRS spectrum of the TiO_2-G material as compared to TiO_2 P25 and TiO_2-G-$NiFe_2O_4$.

reduced and shifted Ti–O–N component (<3% total O species, 528.3 eV).

The N 1s spectra obtained for these materials generally shows a broad peak from 396 to 403 eV, which is typical of nitrogen-doped titanium dioxide (Fig. 7).[11,34] However, in contrast with the similar O 1s spectra found for TiO_2-G and TiO_2-G-$NiFe_2O_4$, the observed N 1s spectra are remarkably different in shape and contribution. After fitting of the curve data, four main peaks were obtained for both magnetically and non magnetically separable materials at *ca.* 400.9, 399.8, 398.9 and 397.6 eV. Generally, two peaks have been reported in N 1s core levels for N-doped TiO_2 materials [11,34,37] The peak at 399.8 eV is attributed to the anionic N- in Ti–O–N, that is, the interstitial N[11,34,38] while the peak at 397.6 eV has been assigned to the substitutional N in O–Ti–N linkages.[11,34,37] The binding energy of the second peak is notably higher than that of TiN appearing at 396.9 eV,[39] which may be due to the higher electron negativity of oxygen than nitrogen, so the electron density on the nitrogen decrease (therefore binding energy increases).

However, due to the peculiar structure of guanidine (which potentially has three N groups available), two alternative bands appeared which are most probably related to the formation of similar Ti–O–N (400.9 eV) and O–Ti–N (398.9 eV) species through binding to the two different types of N (imine and terminal amine groups). These observations are in good agreement with peaks observed in the O 1s spectra and suggest the chemical state of N is primarily as terminal N (interacting with Ti and O in the structure of the material) and not as bulk N doping. The significantly higher binding energies found for the N 1s bands as compared to previous reports (397.6 *vs.* 396 eV) is believed to be due to the strong interaction of the N groups of guanidine with the TiO_2 in a similar way to previous reports, which support the theories on the chemical state of the N species.

Furthermore, these findings were also supported by the results of XPS for the Ti 2p region (not shown). The binding energy of the Ti 2p3/2 core levels of TiO_2-G were found to be 458.4 eV, while pure TiO_2 has been reported to appear at 459.05 eV[34] The binding energy of Ti 2p3/2 after nitrogen doping decreases and suggests different electronic interactions of Ti with anions, which causes partial electron transfer from the N to the Ti and

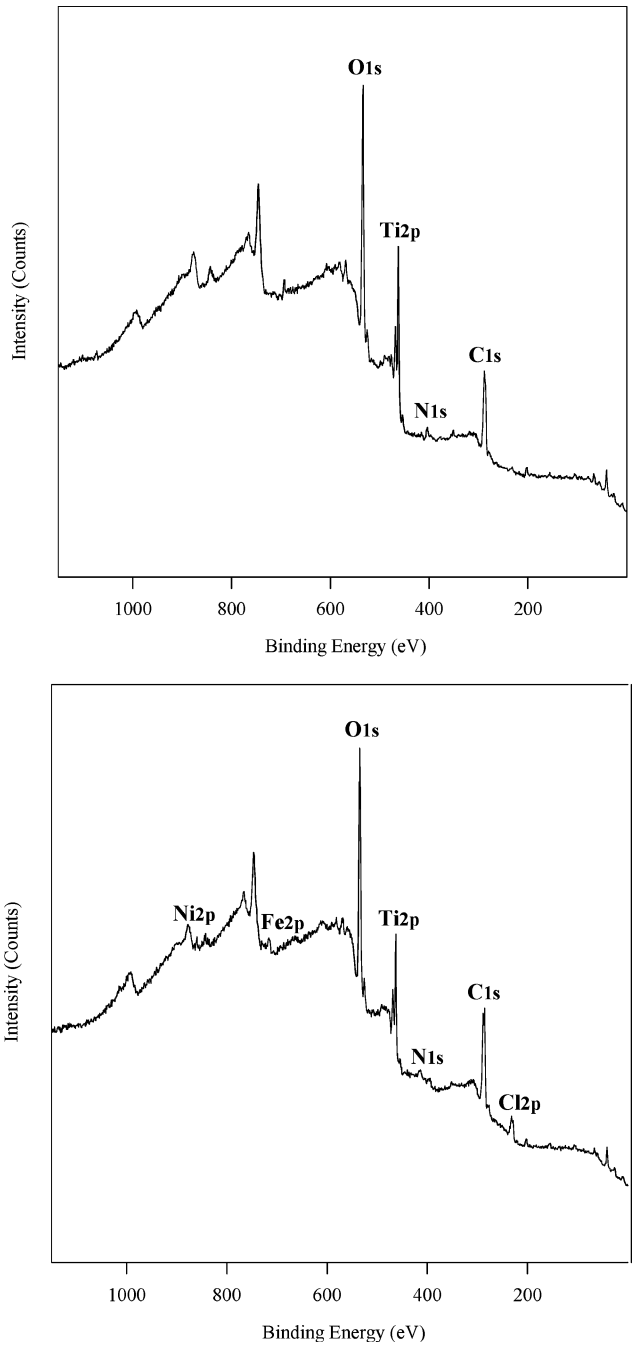

Fig. 5 XPS survey of TiO_2-G material (top) and TiO_2-G-$NiFe_2O_4$ (bottom) materials.

an increase in the electron density of Ti because of the lower electron negativity of nitrogen compared to oxygen. These facts also verified the partial incorporation of nitrogen into the lattice *via* oxygen substitution.

The magnetic properties of the synthesized nanomaterials were also investigated. The magnetization *versus* applied field studies of the Ni and $CoFe_2O_4$ nanoparticles show that the as-synthesized particles are superparamagnetic at room temperature, which is the main criterion for magnetic separation. The saturation magnetization and coercivity of the $NiFe_2O_4$ were found to be 42.24 emu g^{-1} and 12 Oe, respectively. Fig. 8 shows the magnetization *versus* applied field plot

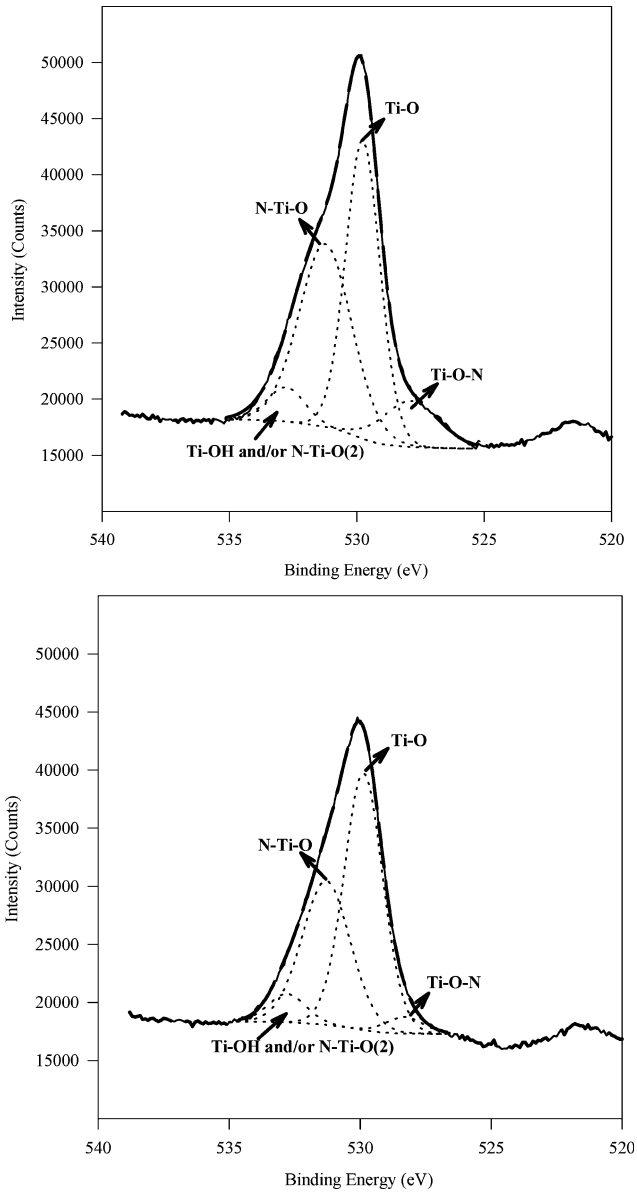

Fig. 6 O 1s XPS of TiO_2-G (top) and TiO_2-G-$NiFe_2O_4$ (bottom) showing the different O species present in the materials.

for the as-synthesized $NiFe_2O_4$. Supported TiO_2-G materials showed similar properties which were in good agreement with their facile magnetic separation by a simple magnet at room temperature.

Characterised materials were subsequently investigated in the photocatalytic transformation of a biomass-derived platform molecule (malic acid, MA) in aqueous solution under visible light. Malic acid (COOH–CHOH–CH_2–COOH) is a C4 dicarboxylic acid that was selected by the USDOE in 2004 as one of the top building blocks to focus at in the near future.[40] Herrmann *et al.* previously investigated the different reaction pathways of this molecule leading to total mineralisation and established a series of parallel degradation routes in which several intermediates (up to 15) were identified prior to achieve total mineralisation of the organic diacid.[30]

Our aim was to selectively obtain some of these intermediates *via* photocatalytic activation avoiding as much as possible total

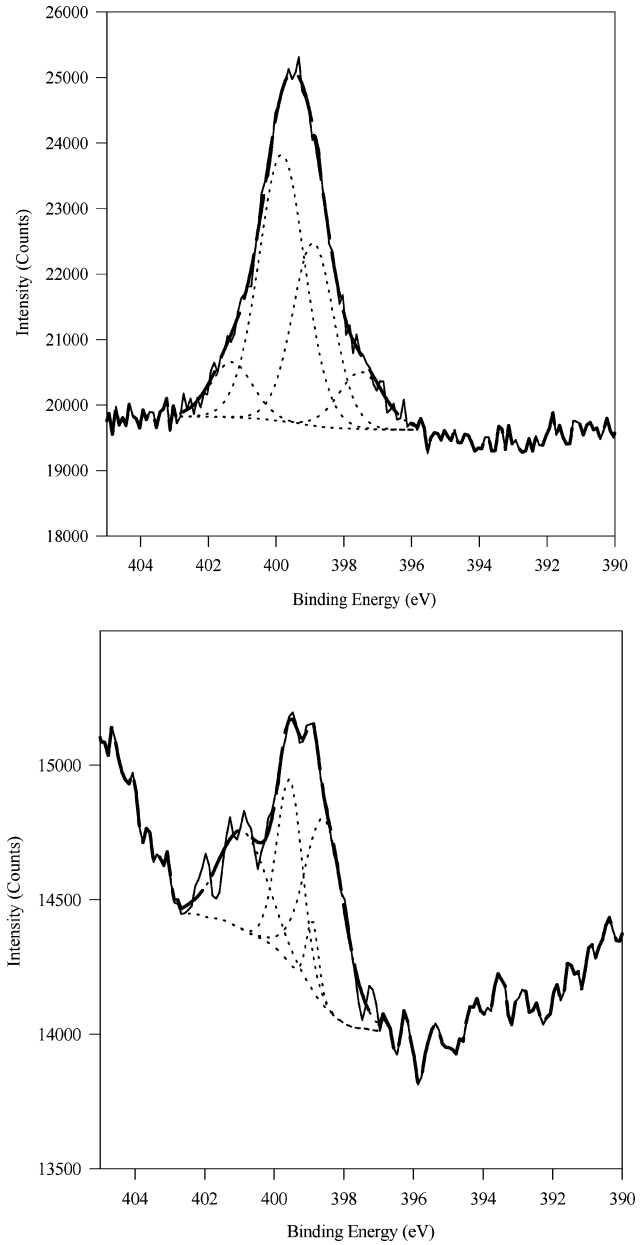

Fig. 7 N 1s XPS of TiO_2-G (top) and TiO_2-G-$NiFe_2O_4$ (bottom) showing the different N species present in the materials.

mineralisation of malic acid. For this, a series of operational parameters known to influence the photocatalytic activity of a material were optimised. These include light intensity, nature and concentration of the substrate, time of irradiation and concentration of the photocatalyst. Optimised results have been included in Fig. 9.

These pointed to the formation of formic (HCOOH) and acetic acids (CH_3–COOH) as main products prior to mineralisation to CO_2 (Scheme 1). Traces of oxalic acid (HCOOH–COOH) were also detected by GC/MS. Under the investigated reaction conditions, a selectivity close to 80% to formic acid could be achieved in less than 2 h of reaction (Fig. 8). The synthesized materials also possessed remarkably improved activities to those of P25 under visible light, with the magnetically separable TiO_2-G-$NiFe_2O_4$ material showing optimum activity at high

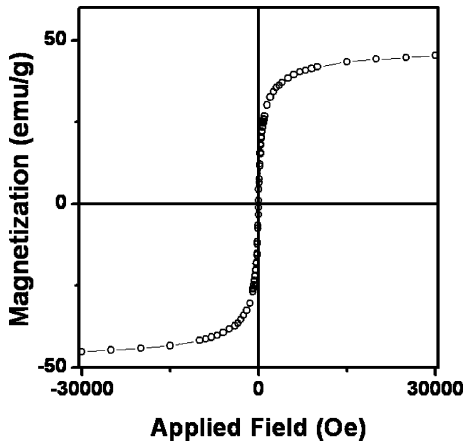

Fig. 8 Magnetization *vs.* applied field magnetic studies of $NiFe_2O_4$.

selectivities. TOC show than less than 15% total mineralisation is obtained under these conditions at times of reaction of 90 min. This high selectivity to formic acid has been reported for the first time. Blank runs (dark experiments) were performed and provided virtually no conversion of starting material under the investigated reaction conditions.

The magnetically separable materials could also be easily separated from the reaction mixture by using a simple magnet, similarly to previous reports by our group,[21,22] and reused in the photocatalytic process several times, preserving almost intact (<90%) its initial activity.

Further experiments are ongoing in our laboratories to complete these results as well as to try to extend this protocol to the production of other intermediates from the degradation pathway from malic acid proposed by Herrmann *et al.* (*e.g.* 3-oxopropanoic acid, acetaldehyde, 2-hydroxypropanoic acid) as well as to related platform molecules (*e.g.* succinic acid). Attempts to extend the protocol to the use of sunlight as irradiation source have also shown a promising results in the degradation of dyes (for instance over a 60% methylene blue degradation after 1 h irradiation on a sunny day). These and other complementary studies will be reported in due course.

4. Conclusions

A series of visible-light effective photocatalysts were synthesized following a simple methodology. Both magnetic and non magnetic materials were found to have various Ti–N environments which in turn rendered useful catalysts to work under visible light and potentially sunlight. Materials were found to be photocatalytically active in the selective transformation of malic acid to high added value compounds, avoiding complete mineralisation. In particular, the magnetically separable catalysts were comparably more active to P25 (used as reference) as well as being easily recoverable from the final solution and recycled several times preserving most of their initial activities. We envisage these materials could also be highly useful for related transformations of biomass-derived platform molecules at mild conditions.

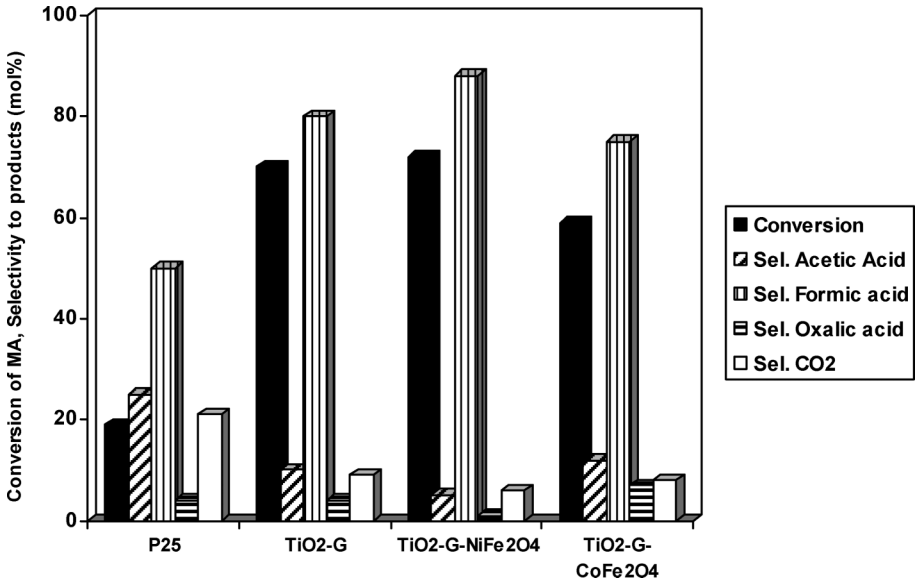

Fig. 9 Photocatalytic transformation studies of malic acid under visible light irradiation using various titania catalysts. Reaction conditions: 0.5 mmol malic acid in 50 mL water, 0.1 g catalyst, 25 °C, 150 W Quartz Halogen Lamp ($\lambda > 400$ nm) irradiation for 90 min.

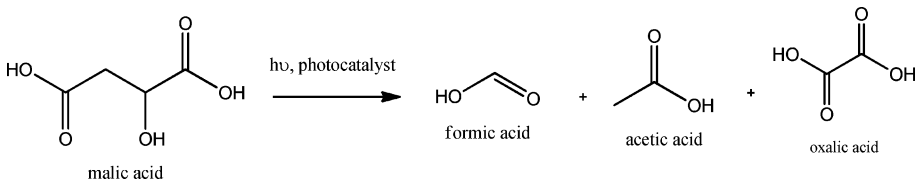

Scheme 1 Photocatalytic transformation of malic acid into different chemicals.

Acknowledgements

Rafael Luque gratefully acknowledges Ministerio de Ciencia e Innovación for the concession of a Ramon y Cajal contract (RYC-2009-04199) and Consejeria de Ciencia e Innovación, Junta de Andalucia for funding under project P10-FQM-6711 as well as for funding a short stay fellowship Incentivos para Actividades de caracter cientifico y tecnico for RL (convocatoria IAC-2010-2) at the EPA in Cincinnati. Elena Serrano acknowledges financial support from Spanish MICINN through the JdC Program (ref. JCI-2008–2165). Alina Balu gratefully acknowledges funds from the research group FQM-162, Departamento de Quimica Organica, Universidad de Cordoba and from Ministerio de Ciencia e Innovacion (Project CTQ 2008-01330/BQU) and Consejeria de Educacion y Ciencia, Junta de Andalucia (Projects P07-FQM-02965 and P09-FQM-4781), co-financed with FEDER funds. BB thanks ORISE for a research fellowship.

References

1 (*a*) *Handbook of Photocatalysts: Preparation, Structure and Applications*, ed. G. K. Castello, Nova Science Publishers, New York, 2010; (*b*) M. Schiavello, *Heterogeneous Photocatalysis*, Kluwer Academic Publishers, Dordrecht, 1997.
2 J. M. Herrmann, *Catal. Today*, 1999, **53**, 115.
3 J. C. Colmenares, R. Luque, J. M. Campelo, F. Colmenares, Z. Karpinski and A. A. Romero, *Materials*, 2009, **2**, 2228.
4 W. A. Zeltner and D. T. Tompkin, *Ashrae Transactions*, 2005, **111**, 532.
5 J. Zhao and X. Yang, *Build. Environ.*, 2003, **38**, 645.
6 O. Carp, C. L. Huisman and A. Reller, *Prog. Solid State Chem.*, 2004, **32**, 33.
7 H. Kim, S. Lee, Y. Han and J. Park, *J. Mater. Sci.*, 2005, **40**, 5295.
8 (*a*) X. Yang, C. Cao, L. Erickson, K. Hohn, R. Maghirang and K. Klabunde, *J. Catal.*, 2008, **260**, 128; (*b*) Z. Lin, A. Orlov, R. M. Lambert and M. C. Payne, *J. Phys. Chem. B*, 2005, **109**, 20948.
9 (*a*) M. Kitano, M. M. Matsuoka, M. Ueshima and M. Anpo, *Appl. Catal., A*, 2007, **325**, 1; (*b*) M. A. Fox and M. T. Dulay, *Chem. Rev.*, 1993, **93**, 341.
10 (*a*) J. Cunningham, G. Al-Sayyed, P. Sedlak and J. Caffrey, *Catal. Today*, 1999, **53**, 145.
11 R. Asahi, T. Morikawa, T. Ohwaki, K. Aoki and Y. Taga, *Science*, 2001, **293**, 269.
12 G. Liu, H. G. Yang, X. Wang, L. Cheng, J. Pan, G. Q. Lu and H. M. Cheng, *J. Am. Chem. Soc.*, 2009, **131**, 12868.
13 H. Yamashita, M. Takeuchi and M. Anpo, Visible light sensitive photocatalysts, *Encyclopedia of Nanoscience and Nanotechnology*, 2004, American Scientific Publishers, California, USA.
14 R. Abe, K. Sayama and H. Arakawa, *J. Photochem. Photobiol., A*, 2004, **166**, 115.
15 (*a*) Z. Jin, X. Zhang, Y. Li, S. Li and G. Lu, *Catal. Commun.*, 2007, **8**, 1267; (*b*) L. C. Chen, C. M. Huang and F. R. Tsai, *J. Mol. Catal. A: Chem.*, 2007, **265**, 133; (*c*) S. Rengaraj and X. Z. Li, *J. Mol. Catal. A: Chem.*, 2006, **243**, 60.
16 (*a*) S. Rehman, R. Ullah, A. M. Butt and N. D. Gohar, *J. Hazard. Mater.*, 2009, **170**, 560; (*b*) R. Asahi and T. Morikawa, *Chem. Phys.*, 2007, **339**, 57; (*c*) Z. Jin, X. Zhang, G. Lu and S. Li, *J. Mol. Catal. A: Chem.*, 2006, **259**, 275.
17 (*a*) Y. Cong, F. Chen, J. Zhang and M. Anpo, *Chem. Lett.*, 2006, **35**, 800; (*b*) N. Serpone, *J. Phys. Chem. B*, 2006, **110**, 24287; (*c*) S. Z. Chu, S. Inoue, K. Wada, D. Li and J. Suzuki, *Langmuir*, 2005, **21**, 8035; (*d*) B. Baruwati and R. S. Varma, *J. Nanosci. Nanotechnol.*, 2011, **11**, 2036.
18 M. H. Habibi, S. Tangestaninejad and B. Yadollahi, *Appl. Catal., B*, 2001, **33**, 57.

19 (*a*) H. Yamashita and M. Anpo, *Curr. Opin. Solid State Mater. Sci.*, 2003, **7**, 471; (*b*) P. F. Fu, Y. Luan and X. G. Dai, *J. Mol. Catal. A: Chem.*, 2004, **221**, 81; (*c*) R. L. Pozzo, M. Baltanas and A. Cassano, *Catal. Today*, 1997, **39**, 219; (*d*) I. M. Arabatzis, S. Antonakari, T. Stergiopoulos, A. Hiskia, E. Papaconstantinou, M. C. Bernard and P. Falaras, *J. Photochem. Photobiol., A*, 2002, **149**, 237.

20 (*a*) V. Polshettiwar and R. S. Varma, *Green Chem.*, 2010, **12**, 743; (*b*) S. Shylesh, V. Schünemann and W. R. Thiel, *Angew. Chem., Int. Ed.*, 2010, **49**, 3428; (*c*) A. H. Lu, E. L. Salabas and F. Schuth, *Angew. Chem., Int. Ed.*, 2007, **46**, 1222.

21 R. Buonsanti, E. Snoeck, C. Giannini, F. Gozzo, M. Garcia-Hernandez, M. A. Garcia, R. Cingolani and P. D. Cozzoli, *Phys. Chem. Chem. Phys.*, 2009, **11**, 3680.

22 R. Buonsanti, E. Carlino, V. Grillo, C. Giannini, F. Gozzo, M. Garcia-Hernandez, M. A. Garcia, R. Cingolani and P. D. Cozzoli, *J. Am. Chem. Soc.*, 2010, **132**, 2437.

23 A. I. Kontos, V. Likodimos, T. Stergiopoulos, D. S. Tsoukleris and P. Falaras, *Chem. Mater.*, 2009, **21**, 662.

24 M. Casavola, R. Buonsanti, G. Caputo and P. D. Cozzoli, *Eur. J. Inorg. Chem.*, 2008, 837.

25 L. Carbone and P. D. Cozzoli, *Nano Today*, 2010, **5**, 449.

26 V. Polshettiwar and R. S. Varma, *Tetrahedron*, 2010, **66**, 1091.

27 R. Luque, B. Baruwati and R. S. Varma, *Green Chem.*, 2010, **12**, 1540.

28 J. Virkutyte, B. Baruwati and R. S. Varma, *Nanoscale*, 2010, **2**, 1109.

29 J. Virkutyte and R. S. Varma, *New J. Chem.*, 2010, **34**, 1094.

30 J. M. Herrmann, H. Tahiri, C. Guillard and P. Pichat, *Catal. Today*, 1999, **54**, 131.

31 R. J. White, R. Luque, V. Budarin, J. H. Clark and D. J. Macquarrie, *Chem. Soc. Rev.*, 2009, **38**, 481.

32 (*a*) A. Kubacka, B. Bachiller-Baeza, G. Colon and M. Fernandez-Garcia, *Appl. Catal., B*, 2010, **93**, 274; (*b*) S. Sato, R. Nakamura and S. Abe, *Appl. Catal., A*, 2005, **284**, 31.

33 (*a*) L. Chen, H. Dai, Y. Shen and J. Bai, *J. Alloys Compd.*, 2010, **491**, L33; (*b*) S. Zhang, H. Niu, Y. Cai, X. Zhao and Y. Shi, *Chem. Eng. J.*, 2010, **158**, 599; (*c*) Z. Zhou, Y. Zhang, Z. Wang, W. Wei, W. Tang, J. Shi and R. Xiong, *Appl. Surf. Sci.*, 2008, **254**, 6972; (*d*) M. Lenglet, F. Hochu, J. Duerr and M. H. Tuilier, *Solid State Commun.*, 1997, **104**, 793.

34 J. Sun, L. Qiao, S. Sun and G. Wang, *J. Hazard. Mater.*, 2008, **155**, 312.

35 (*a*) J. Fang, F. Wang, K. Qian, H. Bao, Z. Jiang and W. Huang, *J. Phys. Chem. C*, 2008, **112**, 18150; (*b*) M. Sathish, B. Viswanathan and R. P. Viswanath, *Appl. Catal., B*, 2007, **74**, 307.

36 Y. Ma, J. Zhang, B. Tian, F. Chen and L. Wang, *J. Hazard. Mater.*, 2010, **182**, 386.

37 Z. Wang, W. Cai, X. Hong, X. Zhao, F. Xu and C. Cai, *Appl. Catal., B*, 2005, **57**, 223.

38 N. C. Saha and H. G. Tompkins, *J. Appl. Phys.*, 1992, **72**, 3072.

39 (*a*) *Handbook of Monochromatic XPS Spectra*, B. V. Christ, John Wiley & Sons, New York, USA, 2000; (*b*) *An introduction to Surface Analysis by XPS and AES*, J. F. Watts and J. Wolstenholme, John Wiley & Sons, Chichester, UK, 2003.

40 http://www1.eere.energy.gov/biomass/pdfs/35523.pdf.